

ALL OPTICAL ACCELERATOR EXPERIMENTS AT LBNL/

W.P. Leemans, D. Rodgers, P.E. Catravas, G. Fubiani, C.G.R. Geddes, E. Esarey, B.A. Shadwick, J. van Tilborg, S. Chattopadhyay, J.S. Wurtele, L. Archambault, M.R. Dickinson, S. DiMaggio, R. Short, K.L. Barat, R. Donahue, J. Floyd, A. Smith, and E. Wong,
Lawrence Berkeley National Laboratory, Berkeley, CA 94720, USA

Abstract

An overview is presented of the status of laser wakefield acceleration research at the OASIS laboratory of the Center for Beam Physics at LBNL. Experiments have been performed on laser driven production of relativistic electron beams from plasmas using a high repetition rate (10 Hz), high power (10 TW) Ti:sapphire (0.8 μm) laser system. Large amplitude plasma waves have been excited in the self-modulated laser wakefield acceleration regime by tightly focusing (spot diameter 8 μm) a single high power (up to 10 TW), ultra-short (< 50 fs) laser pulse onto a high density ($> 10^{19} \text{ cm}^{-3}$) pulsed gasjet of length 1.2 mm. Nuclear activation measurements in lead and copper targets indicate the production of electrons with energy in excess of 25 MeV. This result was confirmed by electron distribution measurements using a bending magnet spectrometer. Progress on implementing the colliding pulse laser injection method is also presented. This method is expected to produce low emittance (< 1.. mm-mrad), low energy spread (< 1%), 40 MeV femtosecond duration electron bunches containing 10^7 electrons/bunch.

1 INTRODUCTION

Laser wakefield acceleration in plasmas [1] offers the potential of developing ultra-compact accelerators capable of producing high quality relativistic electron beams. Acceleration of electrons to energies as high as 100 MeV over mm-size distances has been demonstrated in several experiments [2]-[8]. These energy gains correspond to accelerating electric fields in plasmas greater than 30 GV/m. The excitation of these large amplitude plasma waves was done by operating in the so-called self-modulated laser wakefield acceleration (SM-LWFA) regime [1],[2]-[5].

Under appropriate conditions, it is possible for a single, long laser pulse with duration $L > \lambda_p$ to break up into a train of short pulses, each of which has a width on the order of the plasma wavelength λ_p . Associated with the break up of the long pulse and the formation of the pulse train is a large amplitude plasma wave. In addition to the pulse length criterion, the pulse power P should exceed the critical power $P > P_c$, where, $P_c = 1.7 \cdot 10^{12} \text{ W}$. Since $\lambda_p \gg \lambda_0^{i=2}$ and $P_c \gg \lambda_0^{i=1}$, for fixed laser parameters, the conditions $L > \lambda_p$ and $P > P_c$ can usually be satisfied by operating a sufficiently high plasma density.

/ Work supported by Department of Energy under Contract No.DE-AC-03-76SF0098.

In the SM-LWFA regime the electron beam energy distribution is broad since electrons are trapped from the background plasma in an uncontrolled manner. However, several schemes are currently being pursued using the standard LWFA [1], [6]-[8] (in which $L \dots \lambda_p$) to reduce the energy spread by the use of additional laser injection pulses [9]-[14].

In this article we describe experiments performed at the OASIS laboratory of LBNL [15]-[16] on the SM-LWFA and progress on implementing the LWFA colliding pulse injection method [11]-[14]. The SM-LWFA phase of the experiment has served two purposes: (i) development and commissioning of the laser system, target chamber and various laser beam, plasma and electron beam diagnostics; (ii) production of relativistic electron beams from the SM-LWFA regime at high repetition rate which, in turn, has allowed the first demonstration of radio-isotope production in a lead and copper target. The next phase will aim at producing electron beams in the standard LWFA regime by relying on optical injection using one or two additional laser beams. Section II will describe the experimental set-up. Section III will discuss the nuclear activation experiments and in section IV the summary and conclusions are presented.

2 EXPERIMENTAL ARRANGEMENT

The layout of the experiment is shown in Fig. 1 and consisted of: the high power laser beam, a pulsed gasjet for the plasma source, laser and plasma diagnostics, and electron beam diagnostics.

The high power laser beam was produced with a Ti:Al₂O₃ laser. Pulses from a Kerr lens modelocked Ti:Al₂O₃ oscillator, lasing at about 0.8 μm were first stretched by a grating stretcher with all-reflective optics, to a length of up to 300 ps, controllable through the bandwidth of the injected oscillator pulses. The stretched pulses were amplified in a regenerative amplifier, pumped with a 1 kHz intra-cavity doubled Nd:YLF laser.

The output of the regenerative amplifier, 1.0 - 1.2 mJ per pulse, was sent to a three-pass pre-amplifier, producing about 40 mJ per pulse at a repetition rate of 10 Hz. A fraction of the pulse (8%) was split off and sent to a large aperture five pass main amplifier (AMP1). The rest of the beam was injected into separate amplifier used for laser plasma channeling experiments which are discussed elsewhere [15, 16]. AMP1 brings the beam to an energy of up to 1 J per pulse. This high energy 200-300 ps chirped

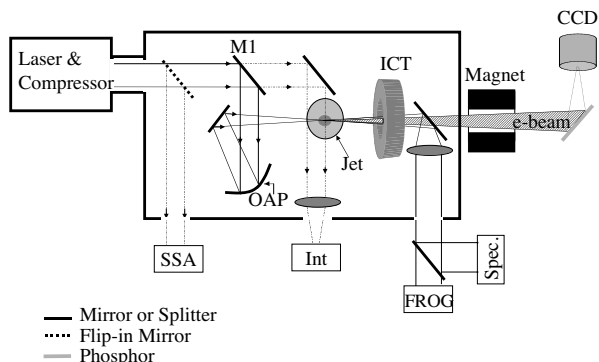


Figure 1: Lay-out of experiment showing the laser beam exiting the compressor, being reflected by mirror M1 onto the off-axis parabola (OAP), which focuses it onto the gasjet. The resulting electron beam is measured using the integrated current transformer (ICT) and is dispersed in the magnetic spectrometer onto a phosphor screen. The screen is imaged with the CCD. Plasma densities are measured with the interferometer (INT) and the laser beam is analyzed using the single-shot autocorrelator (SSA), the frequency resolved optical gating system (FROG) and an imaging optical spectrometer (Spec.).

pulse was propagated into a shielded cave below the laser lab through an evacuated beam pipe. The pulse was then compressed in a vacuum compressor to peak powers of 8-10 TW in a pulse as short as 50 fs. This high power pulse served as the main drive laser pulse for the self-modulated LWFA experiment and will also be the main drive pulse for the upcoming colliding laser wakefield experiments. The peak power of the laser was varied using the pulse duration and laser energy.

The amount and sign of the chirp and, consequently, laser pulse duration, was varied by changing the grating distance in the vacuum compressor. Measurement of the laser pulse duration and laser chirp was done with a commercial single shot autocorrelator (SSA) and a frequency resolved optical gating (FROG) system, respectively. Both systems are located outside the vacuum chamber. To avoid linear and non-linear dispersion effects, the compressor chambers and beam transport tubes were evacuated. A typical compressor scan is shown in Fig. 2(a) and accompanying FROG images in Fig. 2(b).

After compression, the laser beam was reflected with mirror M1 onto an F/4, 30 cm focal length off-axis parabola (OAP), which focused the beam onto a high pressure pulsed gasjet. The gasjet was operated with hydrogen, helium and nitrogen at backing pressures up to 72 bar. OAP alignment was optimized for minimum aberrations, providing a spot size of approximately $8 \mu\text{m}$. A final steering mirror after the OAP was used to provide independent control of the pointing direction. After the interaction region, the main laser beam was reflected by a gold or silver coated $5 \mu\text{m}$ nitrocellulose pellicle. This material and thickness was chosen to minimize Coulomb scattering of electrons

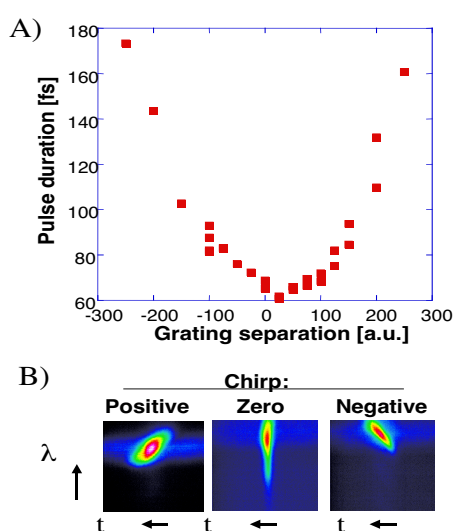


Figure 2: (a) Laser pulse duration vs. compressor grating separation. (b) Spectrum vs. time measured using a frequency resolved optical gating system. The laser chirp sign changes as the pulse compression crosses its minimum value.

propagating through the pellicle, while maintaining optical flatness. After appropriate attenuation, the spectral properties and pulse duration of the exiting laser beam were then analyzed on either a FROG system or an imaging spectrometer.

The density profile of the laser produced plasmas was measured using side-on interferometry of the folded-wave type (figure 3). Laser radiation leaking through M1 was reflected onto a variable optical delay line and sent through the interaction region above the gasjet at right angles to the main beam. After exiting the chamber the probe beam was split and recombined, forming two identical interferograms at the CCD camera. The interaction region was imaged onto the camera using an achromatic lens. Phase changes imparted to the beam by the plasma were extracted from

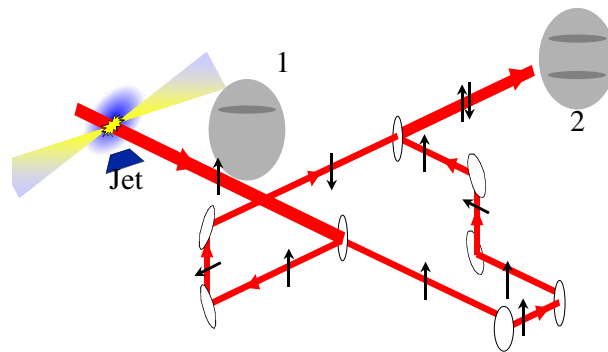


Figure 3: Lay-out of the folded wave interferometer used for measuring the plasma density profile. A single image of the interaction region at (1) is split, folded, and recombined to form two interfering images at the detector (2).

the interferograms, and density profiles were obtained by Abel inverting the two dimensional phase profiles.

The total charge per bunch in the electron beam was measured using a commercial integrating current transformer (ICT). This ICT had been calibrated against a Faraday cup and found to be in very good agreement. The spatial profile was measured with a phosphor screen that was imaged onto a 16 bit CCD camera. The energy distribution of the electron beam was measured by placing the same phosphor and camera downstream of a dipole spectrometer magnet. The ICT as well as an identical magnetic dipole had been previously used at the Beam Test Facility [17], located at the Advanced Light Source of LBNL, with 30 ps long bunches at 50 MeV containing typically 1-1.5 nC.

Neutrons and gamma rays produced during operation of the experiment were monitored with a variety of different detectors, allowing both use of this radiation as a beam diagnostic and the evaluation of various detectors' performance for ultra short radiation pulses [18]. Most of the gamma radiation was produced from the acceleration and deceleration of the electron beam, while neutrons were produced by interactions of high energy gammas with the target. Neutron production therefor served as a rough diagnostic of high energy electron production (fig 4).

The high repetition rate and high power levels sustainable by the I'OASIS laser system produce high energy beams with doses on target sufficient to perform nuclear activation experiments. Nuclear activation through (γ, n) reactions was chosen to provide a lower bound to the electron beam maximum energy. The target material was designed to maximize the high energy Bremsstrahlung yield, generate reaction products with half-life time greater than 5 minutes but shorter than 2 days that emit detectable quantities of characteristic gamma rays, provide incremental indicators over a gamma energy range from 8 MeV to 30 MeV, and be practical to use (available and inexpensive). Candidate elements and reaction products were determined using Refs. [19]-[21].

The electron beam was stopped in a lead/copper target

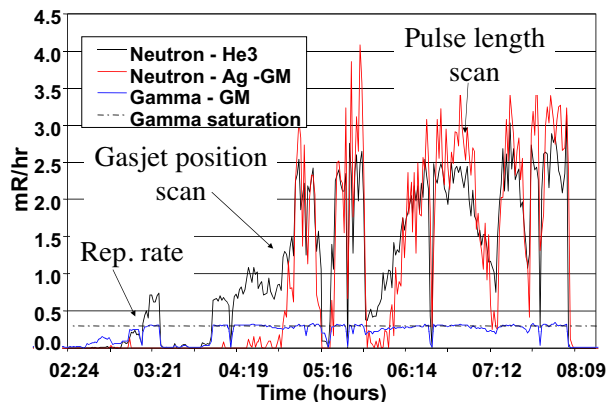


Figure 4: Neutron and Gamma production as a function of time illustrates repeatable, controllable, high energy electron beam production.

and the Bremsstrahlung gamma rays activated the target material. After the target was removed, the reaction products were analyzed by gamma spectroscopy for identification. Transportation to the spectrometer facility meant that counting began fifteen minutes after the beam shut off time. Each reaction, (γ, n), ($\gamma, 2n$), and ($\gamma, 3n$), has a threshold for the energies below which the reaction cannot occur, yielding an unambiguous lower bound on the electron beam energy.

In our experiments, a multi section target constructed of 13 two-piece blocks of various sizes arranged in a bulls eye pattern centered on the beam path approximately 60cm downstream of the gasjet. Each piece was composed of 6.3 mm of Pb at the front and 12.7 mm of Cu at the back. The Cu was selected, because it had all three reactions detectable with a gamma ray energy spread of 10.8 MeV to 31.4 MeV. Pb was chosen to generate Bremsstrahlung photons as well as for the complimentary (γ, n) indicators at 8 and 15 MeV. The choice of thickness of the Pb was a compromise between maximum yield of high energy Bremsstrahlung photons, and minimal absorption before entering the Cu.

3 EXPERIMENTAL RESULTS

Detailed studies of the dependence of electron and neutron production on such parameters as plasma density, laser power, pulselength, chirp, and focal position with respect to the gas jet were made, and nuclear activation experiments in lead and copper were performed.

A typical electron density density profile is shown in Fig. 5. Plasma densities on the order of $1 \text{ } \mu\text{m} \times 5 \times 10^{19}$

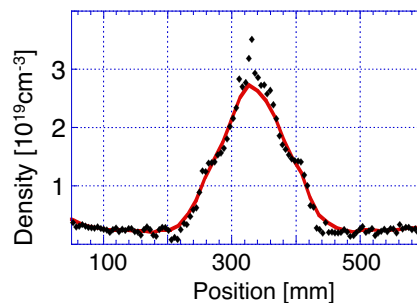


Figure 5: Extracted density profile obtained with the folded wave interferometer. The helium plasma was produced by laser ionization of the gasjet plume.

cm^{-3} were produced, which for multi-TW powers is in the SM-LWFA regime. Generating wakefields in the standard LWFA configuration with such pulses requires a density of $n_0 \sim 5 \times 10^{18} \text{ cm}^{-3}$. Hence, for this laser pulse, the LWFA will be reached by decreasing the plasma density by a factor of 10 compared to the SM-LWFA configuration.

Figure 6 shows laser pulsewidth measured by the SSA along with the blueshifting of the main drive pulse (caused

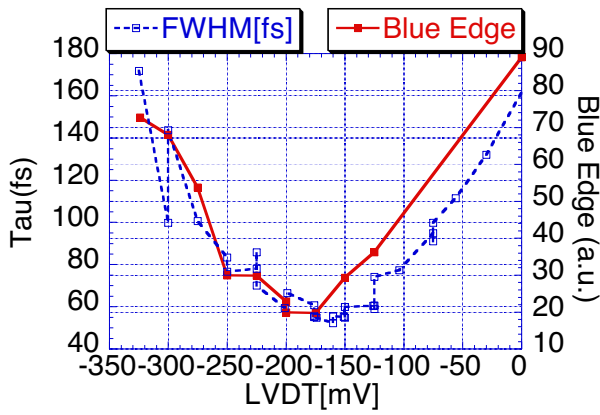


Figure 6: Laser wavelength ionization blueshift and laser pulse duration vs. compressor grating separation.

by the interaction of the laser beam with the rapidly ionizing gas jet plume) as a function compressor grating position. From a one-dimensional ionization blueshifting model it can be seen that the maximum blueshifting occurs at the minimum pulse width due to the fact that the ionization rate, and hence blueshift magnitude, increases with peak laser intensity. Hence the minimum of the blueshift curve indicates the minimum pulsewidth at the interaction point. Note that this minimum occurs at a slightly different position from that measured with the SSA, due to finite temporal dispersion of the exit BK7 window on the vacuum chamber, as well as from the optics of the SSA.

As is evident from Fig. 7, an asymmetry is observed in electron yield measured with the ICT and laser pulse length as a function of compressor grating position. Using the optical imaging spectrometer, spectral sidebands around the center laser wavelength have been observed which also exhibit a similar asymmetric behavior with grating position. As discussed above, the amount and sign of the laser chirp changes while scanning through the compressor minimum. Details of these observations will be discussed in a later paper [22].

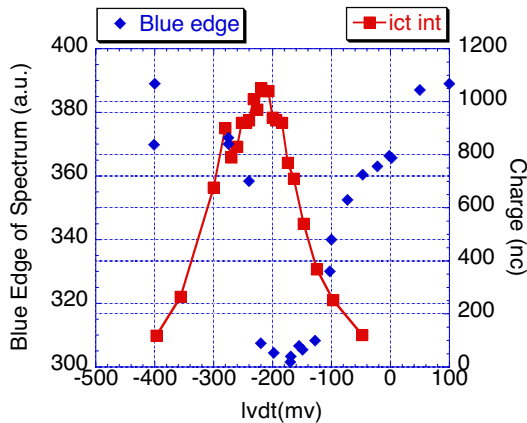


Figure 7: Electron yield in nC and laser pulse duration vs. compressor grating separation.

Electron yield and neutron yields were found to be very well correlated and large increases in yield were observed by adjusting the position of the gasjet edge with respect to the location of the vacuum focus. The yield in electrons and neutrons was also found to scale with increased laser power which will be discussed in a later paper (see Fig. 8).

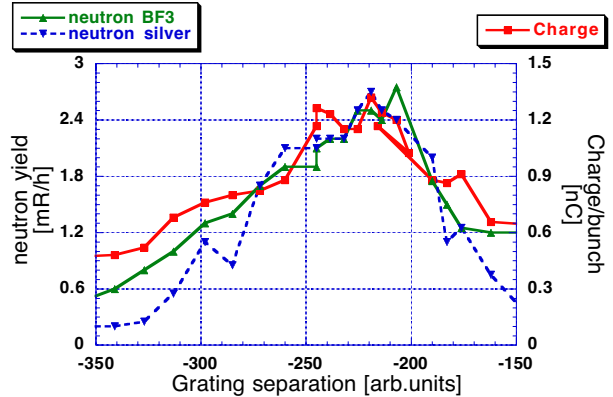


Figure 8: Electron and neutron yield versus compressor position.

For nuclear activation experiments, the target plate was removed from the vacuum chamber after irradiation for 3.5 hours, transferred to the remote counting facility, and individual blocks were removed from the plate for counting. An example gamma spectrum from the counting is shown in fig 9. Initial surveying of the target with a Geiger sur-

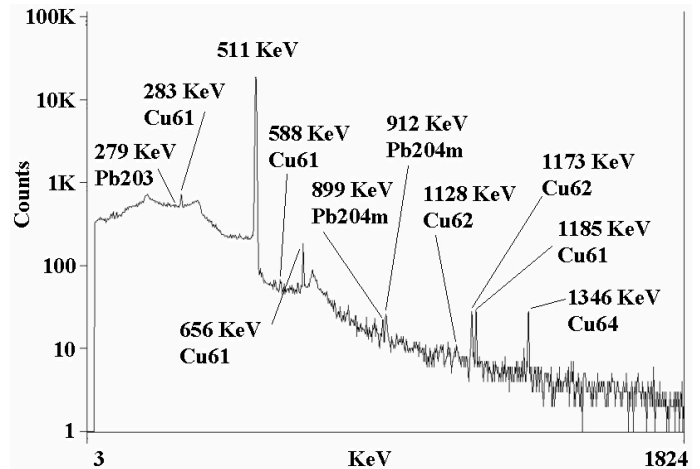


Figure 9: Example gamma ray spectrum from the nuclear activation measurements, showing the peaks corresponding to each isotope produced.

vey meter revealed significant radioactivity on the order of 0.5 μ Ci. The distribution of relative activity on the target was indicative of a well collimated relativistic electron beam emerging from the gasjet, with the majority of all of the activity being from the central 1" diameter block. We identified gamma rays for the ^{63}Cu (γ, n) and ($\gamma, 2n$), ^{65}Cu (γ, n), $\text{Pb}204$ (γ, n), and $\text{Pb}206$ ($\gamma, 2n$) reactions. Successful

observation of the 3.3 hr ^{61}Cu from the $^{63}\text{Cu}(\gamma, n)$ reaction confirmed that the γ -ray (electron) energy distribution had a significant component above 19.7 (25) MeV.

4 SUMMARY AND FUTURE WORK

Recent experiments in the SM-LWFA regime at the L'OASIS laser facility have produced repeatable, high repetition rate electron beams with charge over 1nC and relativistic peak energies over 25MeV. Beam dependence on plasma and laser parameters has been studied, and these measurements will be refined in the near future.

To significantly reduce the energy spread and increase the mean energy, injection of two additional laser pulses is being implemented. Using this method, referred to as the colliding pulse injection method [11, 14], simulations indicate femtosecond duration, relativistic electron bunches (40 MeV in 1 mm) with low fractional energy spread on the order of 1% and low normalized transverse emittance on the order of 1 mm mrad) can be produced. In the simulations, a drive pulse with peak power of 5 TW and colliding pulses of 1 TW each were used. The ponderomotive force of the high-power drive pulse excites a large amplitude wakefield via the standard LWFA mechanism. The two lower power injection pulses collide behind the drive pulse and provide a time-gated electron trapping mechanism by shifting momentum and relative phase of the plasma electrons. Electrons are injected at a very specific phase into the wakefield for acceleration to high energy. This method allows control of the injection process through the injection phase (position of the forward injection laser pulse), beat wave velocity (frequencies of the injection laser pulses), and the beat wave amplitude parameter (injection pulse intensities).

At the present time, new target chambers have been manufactured and installation of optics is in progress. The system is expected to become fully operational during Fall 2000. Since the energy distribution of the electron beam produced with the colliding pulse method is expected to be significantly narrower than what was produced in the SM-LWFA regime, two different magnetic spectrometers have been designed: a low dispersion electromagnet with round poles and a high dispersion square pole magnet using Sm-Co magnets with a surface field strength of 1.1 T. The round and rectangular spectrometers offer broad energy range and good energy resolution, respectively.

5 REFERENCES

- [1] For a review see, E. Esarey, P. Sprangle, J. Krall, and A. Ting, IEEE Trans. Plasma Sci. **PS-24**, 252 (1996).
- [2] A. Modena, Z. Najmudin, A.E. Dangor et al., Nature **377**, 606 (1995); D. Gordon, K.C. Tzeng, C.E. Clayton et al., Phys. Rev. Lett. **80**, 2133 (1998).
- [3] K. Nakajima, D. Fisher, T. Kawakubo et al., Phys. Rev. Lett. **74**, 4428 (1995).
- [4] D. Umstadter, S.Y. Chen, A. Maksimchuk, G. Mourou, and R. Wagner, Science **273**, 472 (1996); R. Wagner, S.Y. Chen, A. Maksimchuk, and D. Umstadter, Phys. Rev. Lett. **78**, 3125 (1997).
- [5] A. Ting, C.I. Moore, K. Krushelnick et al., Phys. Plasmas **4**, 1889 (1997); C.I. Moore, A. Ting, K. Krushelnick et al., Phys. Rev. Lett. **79**, 3909 (1997).
- [6] H. Dewa et al., Nucl. Instr. and Meth. in Phys. Res. A **410** (1998) 357.
- [7] F. Amiranoff et al., Phys. Rev. Lett. **81**, (1998) 995.
- [8] Bernard, D., F. Amiranoff, W.P. Leemans, E. Esarey, and C. Joshi, Nucl. Instr. Meth. A **432**, 227-231 (1999).
- [9] D. Umstadter, J. K. Kim, and E. Dodd, Phys. Rev. Lett. **76**, 2073 (1996).
- [10] R. G. Hemker, K.-C. Tzeng, W. B. Mori, C. E. Clayton, and T. Katsouleas, Phys. Rev. E **57**, 5920 (1998).
- [11] E. Esarey, R. F. Hubbard, W. P. Leemans, A. Ting, and P. Sprangle, Phys. Rev. Lett. **79**, 2682 (1997).
- [12] W. P. Leemans, C.B. Schroeder, P.B. Lee, J.S. Wurtele and E. Esarey, SPIE Conf. Proc. **3451**, San Diego, California, pp. 41-50 (1998).
- [13] C.B. Schroeder, P.B. Lee, J.S. Wurtele, E. Esarey, and W.P. Leemans, Phys. Rev. E **59**, 6037 (1999).
- [14] E. Esarey, C.B. Schroeder, W.P. Leemans, and B. Hafizi, Phys. Plasmas **6**, 2262 (1999).
- [15] W. P. Leemans, P. Volfbeyn, K.Z. Guo, S. Chattopadhyay, C.B. Schroeder, B.A. Shadwick, P.B. Lee, J.S. Wurtele and E. Esarey, Phys. Plasmas **5**, 1615 (1998).
- [16] P.Volfbeyn, E. Esarey and W.P. Leemans, Phys. Plasmas **6**, 2269 (1999).
- [17] W. Leemans et al., Proc. 1993 Part. Acc. Conf., pp. 83 - 85. (1993).
- [18] W.P. Leemans et al, in preparation.
- [19] see <http://ie.lbl.gov/education/isotopes.htm>
- [20] R.E. Sund et al., Phys. Rev. **176**, 1366 (1968).
- [21] S.C. Fultz et al., Phys. Rev. B **133**, 1149 (1964).
- [22] W.P. Leemans et al., in preparation.